Colorimetric Detection Based on Localised Surface Plasmon Resonance Optical Characteristics for the Detection of Hydrogen Peroxide Using Acacia Gum–Stabilised Silver Nanoparticles

Analytical Chemistry Insights
1–10

DOI: 10.1177/1177390116684686

Eman Alzahrani

Chemistry Department, College of Science, Taif University, Taif, Kingdom of Saudi Arabia

ABSTRACT: The use of nanoparticles in sensing is attracting the interest of many researchers. The aim of this work was to fabricate Acacia gum–stabilised silver nanoparticles (SNPs) using green chemistry to use them as a highly sensitive and cost-effective localised surface plasmon resonance (LSPR) colorimeter sensor for the determination of reactive oxygen species, such as hydrogen peroxide (H_2O_2). Silver nanoparticles were fabricated by the reduction of an inorganic precursor silver nitrate solution ($AgNO_3$) using white sugar as the reducing reagent and Acacia gum as the stabilising reagent and a sonication bath to form uniform silver nanoparticles. The fabricated nanoparticles were characterised by visual observation, ultraviolet-visible (UV-Vis) spectrophotometry, transmission electron microscopy (TEM) analysis, energy-dispersive X-ray spectroscopy (EDAX), thermogravimetric analysis (TGA), and Fourier transform infrared spectroscopy (FT-IR). The TEM micrographs of the synthesised nanoparticles showed the presence of spherical nanoparticles with sizes of approximately 10 nm. The EDAX spectrum result confirmed the presence of silver (58%), carbon (30%), and oxygen (12%). Plasmon colorimetric sensing of H_2O_2 solution was investigated by introducing H_2O_2 solution into Acacia gum–capped SNP dispersion, and the change in the LSPR band in the UV-Vis region of spectra was monitored. In this study, it was found that the yellow colour of Acacia gum–stabilised SNPs gradually changed to transparent, and moreover, a remarkable change in the LSPR absorbance strength was observed. The calibration curve was linear over 0.1–0.00001 M H_2O_2, with a correlation estimation (R^2) of .953. This was due to the aggregation of SNPs following introduction of the H_2O_2 solution. Furthermore, the fabricated SNPs were successfully used to detect H_2O_2 solution in a liquid milk sample, thereby demonstrating the ability of the fabricated SNPs to detect H_2O_2 solution in liquid milk samples. This work showed that Acacia gum–stabilised SNPs may have the potential as a colour indicator in medical and environmental applications.

KEYWORDS: Silver nanoparticles, white sugar, Acacia gum, hydrogen peroxide, localised surface plasmon resonance

RECEIVED: September 6, 2016. **ACCEPTED:** November 18, 2016.

PEER REVIEW: Four peer reviewers contributed to the peer review report. Reviewers' reports totaled 1028 words, excluding any confidential comments to the academic editor.

TYPE: Original Research

FUNDING: The author(s) received no financial support for the research, authorship, and/or publication of this article.

DECLARATION OF CONFLICTING INTERESTS: The author(s) declared no potential conflicts of interest with respect to the research, authorship, and/or publication of this article.

CORRESPONDING AUTHOR: Eman Alzahrani, Chemistry Department, College of Science, Taif University, P.O. Box 888, Taif, Kingdom of Saudi Arabia.
Email: em-s-z@hotmail.com

Introduction

Noble metal nanomaterials, such as gold and silver, have attracted the attention of researchers because of their distinctive properties, such as large surface energies, unusual optical properties, chemical stability, good conductivity, and catalytic and antibacterial activity.[1–3] Silver nanoparticles (SNPs) have been used as optical receptors, polarising filters, catalysts, biolabels, and antimicrobial agents.[4,5] Silver nanoparticles can be monitored using a ultraviolet-visible (UV-Vis) spectrophotometer with specific optical characteristics using localised surface plasmon resonance (LSPR) in the visible range (350-800 nm).[6–8]

Localised surface plasmon resonance is excited when electromagnetic radiation interacts with nanoparticles to cause excitation of the conduction electrons. Previous works have shown that LSPR was affected by the composition, size, and shape of SNPs.[9] Localised surface plasmon resonance has been used to monitor bimolecular interactions, for example, enzymatic reactions,[10] DNA hybridisation,[11,12] and antigen-antibody reactions.[13]

Hydrogen peroxide (H_2O_2) is formed in living organisms as a by-product of oxygen metabolism, and it plays an important role in oxidative stress as a reactive oxygen species (ROS). Hydrogen peroxide can be formed by enzymatic reaction; hence, this method can be used to measure target molecules, such as glucose, alcohol, and lactates, based on enzymatic reaction.[14] Previous studies using the LSPR-based optical method with SNPs to monitor target molecules in medical applications are limited in the literature, although there are a few such studies.[15,16] Filippo et al[17] monitored LSPR optical characteristics and dispersion condition changes for the determination of H_2O_2 using polyvinyl alcohol–capped SNPs. In addition, Endo et al[18] used polyvinylpyrrolidone-stabilised SNPs as an LSPR colorimetric sensor for monitoring H_2O_2. Tashkhourian et al[19] determined H_2O_2 using LSPR optical characteristics with SNPs. A recent experimental study from Shrivas et al[16] fabricated SNPs capped with tartaric acid to use them as an LSPR sensor for monitoring chromium.

Silver nanoparticles have been synthesised using chemical stabilising reagents, such as sodium citrate, ascorbate, and sodium borohydride,[20–22] by photo-reduction in reverse micelles[23] and by radiation-chemical reduction.[24] Many of

these methods are of high cost and need to use temperature, pressure, energy, or toxic chemicals, and they are not easily scaled up for the large-scale fabrication of nanoparticles.[25] In addition, toxic chemicals used could be absorbed on the surface of the SNPs, thus limiting their application. Other methods that can be used for the fabrication of SNPs are biological methods based on using microorganisms,[26,27] enzymes,[28] or fungus[29]; however, these methods need special culture preparation and isolation methods for the fabrication of SNPs.[30,31] A green chemistry route for the fabrication of SNPs would have many advantages compared with other methods, such as facile fabrication, environmentally friendly, elimination of the need for any special culture preparation and isolation method, low cost, low yields, easy scaling up for the large-scale fabrication of nanoparticles, and not consuming a lot of energy.[1,31–34]

To the best of our knowledge, there are only a limited number of papers in the literature on using SNPs as a colorimeter sensor for the determination of H_2O_2; therefore, the purpose of this research was to detect H_2O_2 solution based on LSPR using Acacia gum–stabilised SNPs as a model case. Silver nanoparticles were fabricated using an eco-friendly method to avoid using toxic or hazardous chemicals. The fabrication was performed using white sugar as a reducing reagent for the silver nitrate salt ($AgNO_3$) and Acacia gum as a stabilising reagent to fabricate SNPs under ultrasound irradiation and with alkalisation of the reaction by adding sodium hydroxide (NaOH). The prepared materials were characterised using transmission electron microscopy (TEM), energy-dispersive X-ray analysis (EDAX), Fourier transform infrared spectroscopy (FT-IR), and thermogravimetric analysis (TGA). The LSPR optical characteristics to detect H_2O_2 using Acacia gum–stabilised SNPs were evaluated using a UV-Vis spectrophotometer. In addition, the calibration characteristics of this detection method were evaluated.

Experimental

Chemicals and materials

Commercially available white sugar, Acacia gum, and liquid milk samples (Almarai and Alsafi) were purchased from a local supermarket in Taif, KSA. Analytical grade $AgNO_3$ (99.8%) was purchased from Sigma-Aldrich (Nottingham, UK). Hydrogen peroxide (30% [v/v]) was purchased from Acros Organics (Loughborough, UK). Sodium dihydrogen phosphate and disodium hydrogen phosphate for phosphate buffer preparation were purchased from Sinopharm Chemical Reagent Co., Ltd (Beijing, China). All the chemicals were used without any further purification. Solutions were prepared using distilled water and were used for all the preparations.

Instrumentation

The bath sonicator (100 W, 42 kHz) and magnetic stirrer and heater were purchased from Fisher Scientific Co. Ltd. (Shanghai, China). The TEM instrument came from JEOL Ltd. (Welwyn Garden City, UK). The EDAX analysis was obtained using a JEOL JSM 6390 LA Analytical device (Tokyo, Japan). The UV-Vis spectrophotometer was from Thermo Scientific GENESYS 10S (Toronto, Canada). The FT-IR spectra were collected in the attenuated total reflectance (ATR) mode using a PerkinElmer RX FT-IR 2× instrument with diamond ATR and DRIFT attachment from PerkinElmer (Buckinghamshire, UK). The thermogravimetric analyser was from TA Instruments (New Castle, DE, USA).

Synthesis of Acacia gum–stabilised SNPs

The reaction was performed in a sonicator at an operating power output of 100 W and at a frequency of 42 kHz while the temperature was kept constant at 35 ± 2°C in the sonicator. Sixteen millilitres of Acacia gum (0.2%) was added to 8 mL of $AgNO_3$ (1 mM) for 10 minutes. Then, 24 mL of white sugar solution (0.1 M) and 1.5 mL of NaOH solution (0.1 M) were added to the mixture. The fabricated SNP solutions were stored at 2°C and were utilised within 1 week. For comparison, Acacia gum–stabilised SNPs were fabricated using a different agitation method (mechanical or magnetic stirring) with the same chemicals and procedure.

Characterisation of the fabricated SNPs

UV-Vis spectroscopy. Besides the colour of the solution, which was observed by naked eye to check the formation of SNPs, the fabricated Acacia gum–stabilised SNP solution was monitored using a UV-Vis spectrophotometer. The absorbance of 1 mL of sample solution was measured using a UV-Vis spectrophotometer and compared with 1 mL of distilled water as a blank over the range of 350 to 800 nm operated at a resolution of 1 nm.

TEM analysis. The formation of Acacia gum–stabilised SNPs was studied using TEM analysis. For this, 5 µL of the sample solution was put onto lacy carbon-coated 3 mm diameter copper grids. Transmission electron microscopy images were acquired with a Gatan Ultrascan 4000 digital camera attached to a JEOL 2010 transmission electron microscope running at 20 kV. The size of the prepared nanoparticles was measured using Image J software.

EDAX analysis. The fabricated Acacia gum–stabilised SNPs were separated by centrifuging at 1100 rpm for 15 minutes. Energy-dispersive X-ray analysis was used to obtain the chemical composition of the fabricated materials.

FT-IR analysis. An FT-IR spectrum was obtained using an FT-IR spectrophotometer in a wavenumber range of 4000 to 500 cm^{-1} with a resolution accuracy of 4 cm^{-1}. The sample was ground and mixed with KBr in a ratio of 1:100. Then, they were pressed to make transparent thin pellets. The spectrum was recorded in the transmittance mode as a function of the wavenumber.

TGA analysis. Thermal characterisation was performed using a thermogravimetric analyser at a heating rate of 10°C min^{-1} in a nitrogen environment and held for 1 minute at 25°C. Fabricated material of 10 mg was heated in an alumina crucible and the TGA profile was recorded from 25°C to 600°C at a scan rate of 10°C min^{-1}.

Detection of H_2O_2 based on the LSPR-based ROS detection method

The experimental conditions for the LSPR-based ROS detection method using Acacia gum–stabilised SNPs were as follows: 2 mL of different concentrations of H_2O_2 solution prepared using 20 mM phosphate buffer (pH 7.0) was mixed with 3 mL of Acacia gum–stabilised SNPs. Then, the solution mixture was kept at a room temperature of 25 ± 3°C. The change in the optical characteristics of the LSPR-based ROS detection procedure was carried out using a UV-Vis spectrophotometer over the range of 350 to 800 nm at room temperature. In addition, H_2O_2 solution containing the Acacia gum–stabilised SNPs was utilised for TEM observation.

Results and Discussions

Formation of Acacia gum–stabilised SNPs

In this study, SNPs stabilised with Acacia gum were prepared using wet chemical synthesis because it is the most common procedure for the fabrication of uniform nanoparticles of precisely controlled sizes and stable SNPs and their colloidal dispersions in water or organic solvents.[35–37] The reduction was performed under a sonication bath or stirrer using non-toxic and environmentally friendly reducing reagent, namely, white sugar, which was responsible for the reduction of silver ions (Ag^+) to colloidal SNPs (Ag^o), and a non-toxic capping agent, namely, Acacia gum, for size stabilisation of the nanoparticles and to avoid their agglomeration, sedimentation, or loss of surface properties.[38] Moreover, NaOH solution was added to fabricate uniform size and shaped nanoparticles.[39]

Characterisation of Acacia gum–stabilised SNPs

Optical studies. It is well known that the reduction of silver ions into SNPs is commonly followed by a colour change so that the formation of SNPs can be visually observed. Therefore, the change in colour was visually monitored to check for the formation of SNPs and the reaction was stopped when there was no additional change in the solution colour.[40–42] Figure 1A shows that the colour of the reaction mixture prepared using a sonication bath or stirrer gradually changed from colourless to brown within 30 minutes due to the formation of SNPs in the solution. In addition, it was observed that there was a difference in the colour of the prepared SNPs using a sonication bath compared with a stirrer.

The effect of the agitation method on the fabricated SNPs was studied using UV-Vis spectrophotometer because SNPs can absorb light in the visible region due to the surface

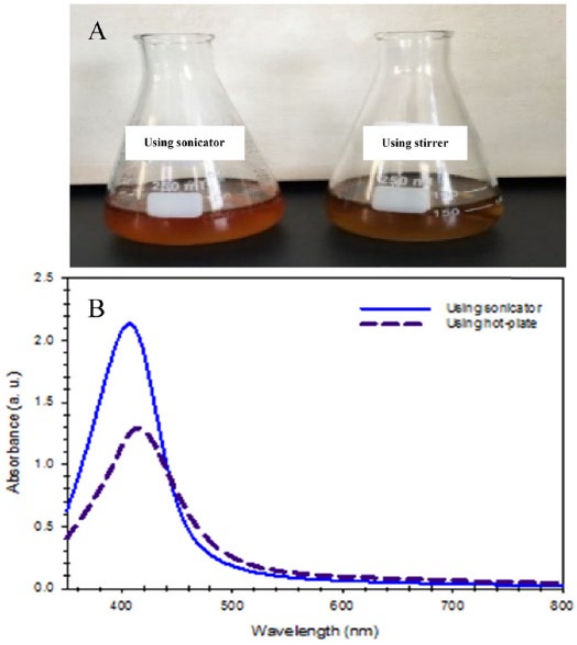

Figure 1. (A) Change in the colour of the silver nitrate solution after the reduction of silver ions and the formation of silver nanoparticles (SNPs) under ultrasound irradiation (left) and magnetic stirring (right). (B) Comparison between the UV-visible absorption spectra of the fabricated SNPs using different agitation methods.

plasmon resonance phenomenon based on their size and shape.[43–45] Figure 1B shows the UV-Vis spectra of the Acacia gum–stabilised SNPs prepared under ultrasound and magnetic stirring. It was found that the absorbance peak of SNPs prepared using the sonication bath was higher than the absorbance peak of SNPs prepared using a stirrer. This result indicated that there was a greater reduction of silver ions and a greater formation of SNPs when using a sonication bath, indicating that using ultrasound irradiation can enhance the rate of reaction. In addition, the full peak width at half maximum (FWHM) was calculated, and it was found that the FWHM of SNPs prepared using a stirrer was 90 nm and the large FWHM was due to peak broadening and polydispersity,[46] whereas for SNPs prepared using a sonication bath, the FWHM was 75 nm, indicating the formation of uniform SNPs when using a sonication bath.

The maximum absorbance peak of SNPs prepared using the sonication bath was 407 nm, which means there was a slight blue shift compared with the common maximum absorbance peak of the SNPs of 410 to 422 nm.[47–49] The results are in accordance with the data reported in the literature, which shows a blue shift of the maximum absorbance peak (408 nm) of starch-stabilised SNPs prepared using D-glucose under sonication irradiation.[39] So far, there is no general rule for the shift of the SNP band. However, the shift of the band could be due to the difference in size, shape, and dielectric environment.[50,51] Following these results, all further work in this study was performed in a sonication bath for the preparation of Acacia gum–stabilised SNPs.

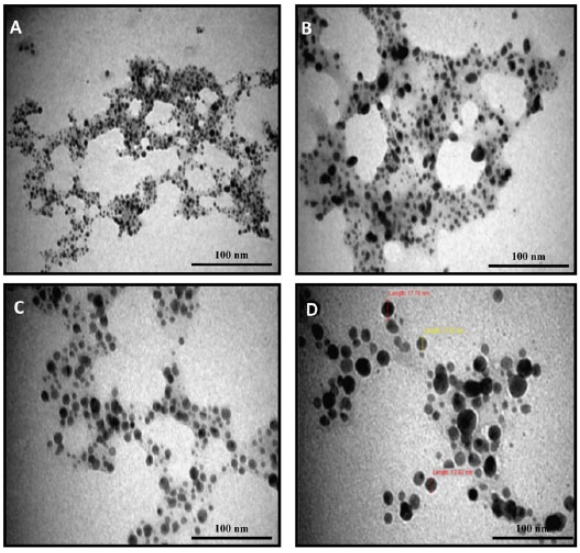

Figure 2. Transmission electron microscopy micrographs of the synthesised Acacia gum–stabilised silver nanoparticles using different magnifications: (A) ×100, (B) ×150, (C) ×250, and (D) ×400.

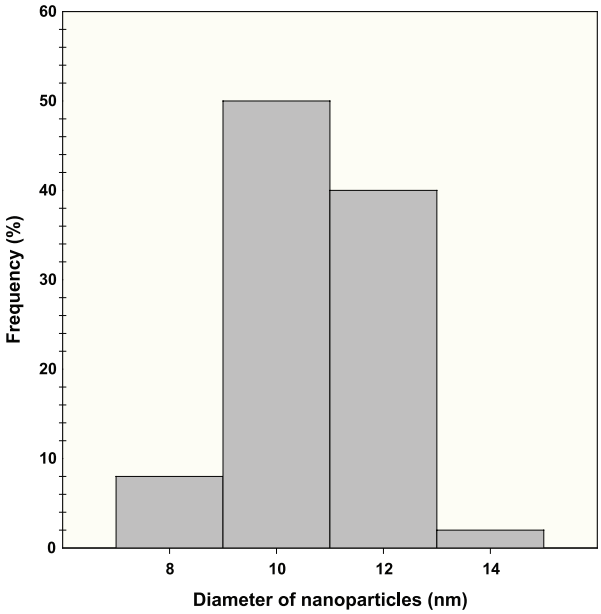

Figure 3. Histogram showing the range of silver nanoparticle size distribution.

Morphological characterisation and pore size studies. In this study, the fabricated Acacia gum–stabilised SNPs were characterised using TEM analysis, which can provide information about the morphology and size of fabricated nanoparticles.[8,52] Figure 2 shows the TEM micrographs of the fabricated Acacia gum–stabilised SNPs, using different magnifications. It was observed that the fabricated SNPs were in the nano range and were well dispersed without aggregation, possessing a spherical shape. The corresponding particle distribution histogram of the fabricated SNPs is shown in Figure 3. It was found that the average size distribution was 10 nm, with a standard deviation of 6 nm.

EDAX analysis. Energy-dispersive X-ray spectroscopy analysis can provide qualitative and quantitative data of the elements of fabricated materials. Therefore, the fabricated Acacia gum–stabilised SNPs were studied using EDAX analysis. Figure 4 shows the EDAX spectrum, displaying the elemental composition of the sample. As can be seen in the middle of the EDAX spectrum, there are 3 peaks located between 2 and 4 keV, related to silver's characteristic lines K and L, and an optical absorption peak at 3 keV because of surface plasmon resonance.[53–55] This revealed that the nanostructure was formed of silver. In addition, other elements can be observed on the left part of the EDAX spectrum, namely, carbon (C) at 0.2 keV and oxygen (O) at 0.5 keV. The appearance of carbon and oxygen peaks in the tested samples confirms the presence of the stabiliser. The same result was obtained by other groups.[56]

The EDAX spectrum obtained was used for carrying out the quantitative analysis. It was found that there were high silver contents (58 %) in the examined samples, whereas the contents of carbon and oxygen were 30% and 12%, respectively. The obtained result from the EDAX analysis confirmed the formation of SNPs without impurities.

FT-IR measurement. Fourier transform infrared spectroscopy was carried out to identify the possible Acacia gum responsible for capping, which can increase the stability of SNPs in the colloids. Figure 5 shows the FT-IR spectrum of the fabricated Acacia gum–stabilised SNPs. The intense broad band at 3400 cm^{-1} can be assigned to O-H, stretching vibrations of carboxylic acid and hydroxyl groups. The absorption band at 1660 cm^{-1} corresponds to C=O stretching, which is attributed to polyccarides.[57] The two bands at 1422 and 1364 cm^{-1} that are common bands for Acacia gum were not observed. This could be due to the stabilisation of SNPs by hydroxyl bond deformation at the silver metal surface. A similar result was obtained by Rao et al.[58]

Thermal properties of Acacia gum–stabilised SNPs. The thermal properties of Acacia gum–stabilised SNPs were studied by TGA under a nitrogen atmosphere held for 1 minute at 25°C. Ten milligrams of the SNPs was heated in alumina crucibles and the TGA profile was recorded from 25°C to 600°C at a scan rate of 10°C min^{-1}. The thermogram of Acacia gum–stabilised SNPs is depicted in Figure 6. As can be seen, an initial weight loss can be observed in the temperature range of 30°C to 200°C. This might be due to the desorption of bound water molecules and adsorbed species present in the Acacia gum–stabilised SNPs.[59] The second step (above 200°C) was due to the thermal degradation of the Acacia gum capping around the SNPs to carbon residue.[60]

Evaluation of the Acacia gum–stabilised SNPs as an LSPR-based optical H_2O_2 sensor

The calibration characteristics of H_2O_2 using the Acacia gum–stabilised SNPs as an LSPR-based optical sensor were studied. This was performed by adding 0.001 M H_2O_2 prepared using 20 mM phosphate buffer solution (pH 7.0) to the Acacia gum–stabilised SNPs at a volume ratio of 1:1.5. As can be seen in Figure 7A, bubbles were observed in the solution placed in the

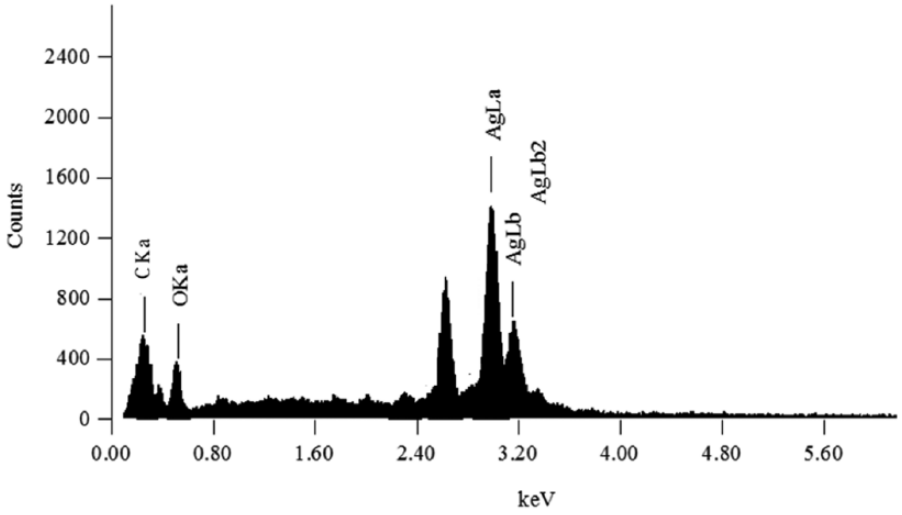

Figure 4. Energy-dispersive X-ray spectroscopy characteristic spectrum of the fabricated Acacia gum–stabilised silver nanoparticles.

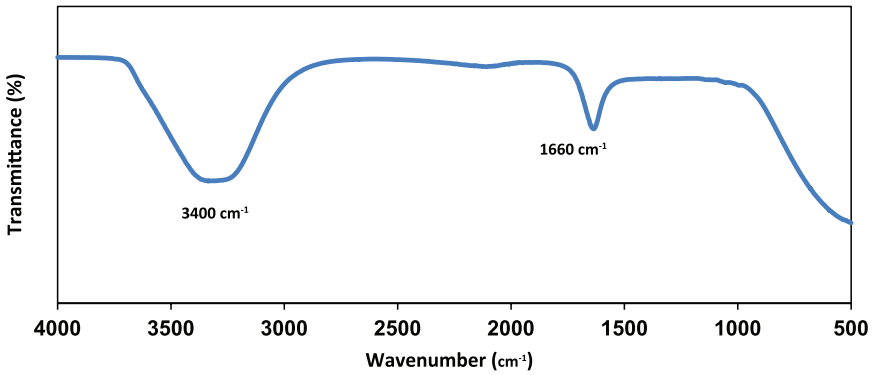

Figure 5. Fourier transform infrared spectroscopy transmittance spectrum of the fabricated Acacia gum–stabilised silver nanoparticles.

cuvette after 1 minute of adding 0.001 M H_2O_2 solution. The reason for the formation of bubbles in the solution was due to the decomposition of H_2O_2 by the catalytic reaction between H_2O_2, which is strong oxidising reagent, and the Acacia gum–stabilised SNPs and the subsequent formation of oxygen molecules,[61] as can be seen in the following formula that describes the reaction of SNPs with H_2O_2 solution and the transformation of SNPs into silver ions[62–64]:

$$Ag + 2H_2O_2 \rightarrow Ag^+ + O_2 \uparrow + 2H_2O \ \Delta E^\circ = 0.067$$

The change in the optical characteristics of the LSPR-based optical H_2O_2 sensor with time (1, 4, 8, 12, 16, 20, 30, 40, 50, 60, 70, 80, 90, and 120 minutes) in the visible range (350-800 nm) was monitored. Figure 7B presents the change in the LSPR optical characteristics with time. As can be seen, there was a significant decrease in the absorbance strength at λ_{max} after 1 minute of adding H_2O_2 solution from 1.880 to 0.872 because of the catalytic reaction between the Acacia gum–stabilised SNPs and 0.001 M H_2O_2 solution. Moreover, there was a red shift of the spectrum band of the Acacia gum–stabilised SNPs to 419 nm after adding the H_2O_2 solution. The reason for the decrease in the absorbance strength and the shift of the LSPR band maximum was because of the destruction of the end capping shell (Acacia gum) resulting in the aggregation of SNPs and a decrease in the distance between the particles. In addition, the catalytic decomposition of H_2O_2 was accomplished with the degradation of SNPs by oxidation of the SNPs by the strong oxidising agent (H_2O_2), resulting in the conversion of Ag^o to silver ions (Ag^+).[18,39,65] These results showed that the change of the absorbance strength at λ_{max} of the LSPR spectrum band can be used as a sensitive signal for fast colorimetric detection of H_2O_2 solution.

Quantitative determination of H_2O_2

For quantitative determination of the H_2O_2 concentration using the Acacia gum–stabilised SNPs, different concentrations of H_2O_2 solution (0.5-0.00001 M) prepared using 20 mM phosphate buffer solution (pH 7.0) were added to Acacia gum–stabilised SNPs at a volume ratio of 1:1.5, and the UV-Vis absorption spectra were recorded after 60 minutes of adding H_2O_2 solution to evaluate the calibration characteristics. Figure 8A shows a photograph of the Acacia gum–stabilised SNPs after introducing different concentrations of H_2O_2 solution showing the change in colour of the Acacia gum–stabilised

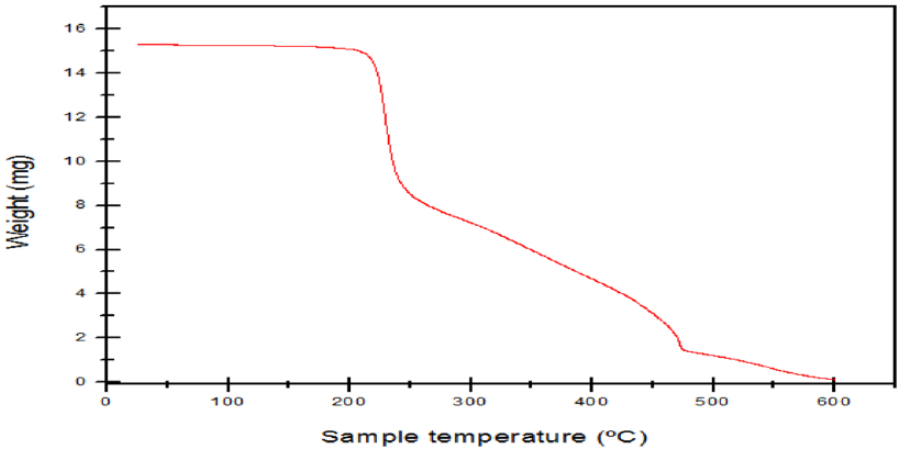

Figure 6. TGA thermogram of the fabricated Acacia gum–stabilised silver nanoparticles.

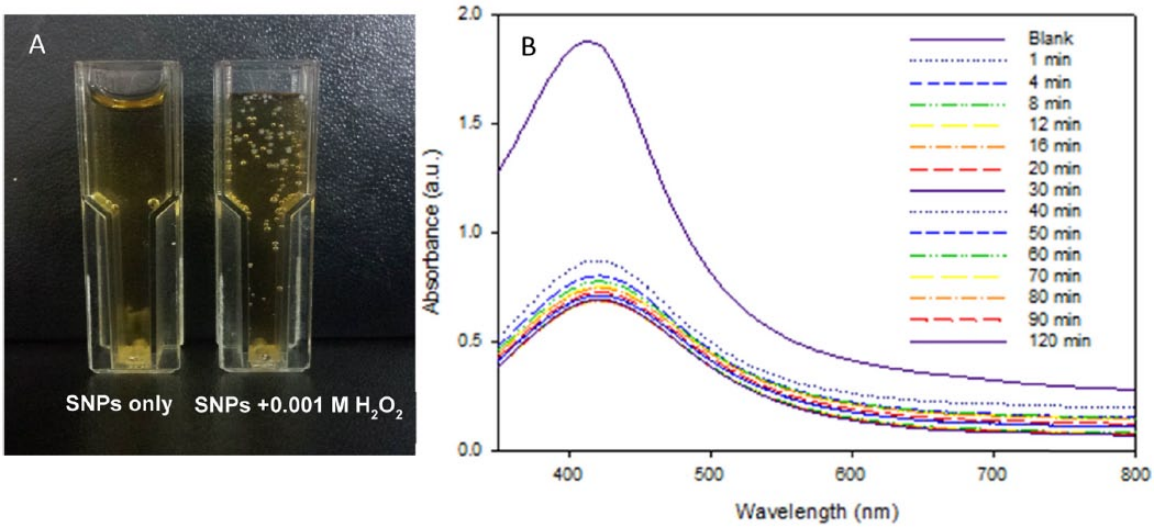

Figure 7. (A) Image showing the bubbles due to the decomposition of H_2O_2 solution generated by the catalytic reaction between H_2O_2 solution and the Acacia gum–stabilised silver nanoparticles (SNPs) after 1 minute of the addition of H_2O_2 solution. (B) Localised surface plasmon resonance optical characteristics change with time due to the addition of H_2O_2 solution (0.001 M) in the prepared Acacia gum–stabilised SNPs at a volume ratio of 1:1.5.

SNPs from yellow by LSPR absorption to transparent. The change of the solution colour was due to the aggregation of SNPs induced by H_2O_2 solution.[66] A higher concentration of H_2O_2 solution causes a higher aggregation and a colour change of SNPs that can observed by the naked eye, with the colour change being directly proportional to the amount of H_2O_2 solution added to Acacia gum–stabilised SNP solution.

As there was a change in the colour of the Acacia gum–stabilised SNP solution, the LSPR optical characteristic change with time could be monitored with a UV-Vis spectrophotometer. The relationship between the change of LSPR absorbance strength and the concentration of H_2O_2 solution can be seen in Figure 8B. It is obvious that there was a remarkable change in the LSPR absorbance strength, which depended on the concentration of H_2O_2 solution. This resulted from the catalytic decomposition of H_2O_2 solution inducing the aggregation of the Acacia gum–stabilised SNPs, thus resulting in a higher decrease in the absorbance of the Acacia gum–stabilised SNPs; a similar result was obtained by other groups.[17,67]

To make sure that the LSPR absorbance strength change was caused by the catalytic reaction between H_2O_2 and the Acacia gum–stabilised SNPs only, distilled water mixed with 20 mM phosphate buffer solution (pH 7.0) was added to the Acacia gum–stabilised SNPs at a volume ratio of 1:1.5, and the experiment was rerun. It was found that there was no change in the LSPR absorbance strength, thus confirming that the decomposition of SNPs was due to adding H_2O_2 solution.

Linear range and precision

The kinetic curves at different concentrations of H_2O_2 solution, in the range between 0.5 and 0.00001 M, added to the

Acacia gum–stabilised SNPs with time were studied to evaluate the analytical applicability of the fabricated SNPs as an LSPR-based sensor. Figure 9 shows the relationship between absorbance strength change and time for different H_2O_2 concentrations. The relative change of the absorbance strength was presented as the ratio $(A_o - A_t)/A_o$, where A_o and A_t are the absorbance of the Acacia gum–stabilised SNPs only and the absorbance of the Acacia gum–stabilised SNPs after adding H_2O_2 solution at different times, respectively. The ratio $(A_o - A_t)/A_o$ was proportional to the degree of conversion of the catalytic reaction between the H_2O_2 solution and Acacia gum–stabilised SNPs.

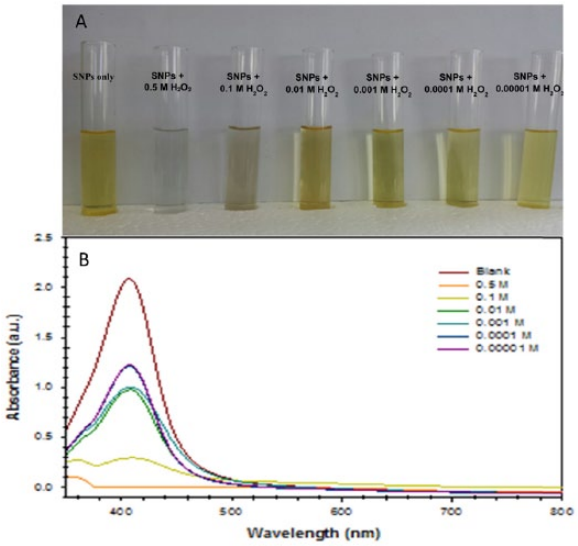

Figure 8. (A) Photograph of a test tube containing Acacia gum–stabilised silver nanoparticles (SNPs) with different concentrations of H_2O_2 solution (0.5-0.00001 M) showing the change in the solution colour of Acacia gum–stabilised SNPs after 60 minutes of reaction time at room temperature. (B) Localised surface plasmon resonance optical characteristics change with time due to the aggregation of SNPs induced by H_2O_2 solution.

The linear range and precision using Acacia gum–stabilised SNPs as an LSPR-based chemical sensor for the colorimetric detection of H_2O_2 were investigated. Figure 10 presents the relationship between the change in the absorbance strength and the concentration of H_2O_2 solution at a reaction time of 15 minutes. A linear response of the Acacia gum–stabilised SNPs as a function of H_2O_2 solution concentration can be seen, with the linear range of 0.1 to 0.00001 M and a correlation of estimation R^2 of .953, thus confirming that the fabricated SNPs are suitable for colorimetric detection of the oxidising reagent (H_2O_2).

The within-batch and between-batch precision of the procedure was investigated as the relative standard deviation (RSD) by calculating the intraday and interday precision (n = 3) of the analysis of 0.001 M H_2O_2 in triplicate analyses (Table 1), and it was found to be between 3.1% and 4.7% for the intraday precision and between 3.5% and 6.4% for the interday precision. Therefore, this method was reproducible for the determination of H_2O_2 solution.

TEM imaging for evaluation of the Acacia gum–stabilised SNPs

The fabricated Acacia gum–stabilised SNPs were examined by TEM analysis after adding H_2O_2 solution. As can be seen in Figure 11, it was observed that the morphology of the Acacia gum–stabilised SNPs was completely changed after introducing H_2O_2 solution and the spherical colloids could not been seen, compared with Figure 2. Before adding H_2O_2

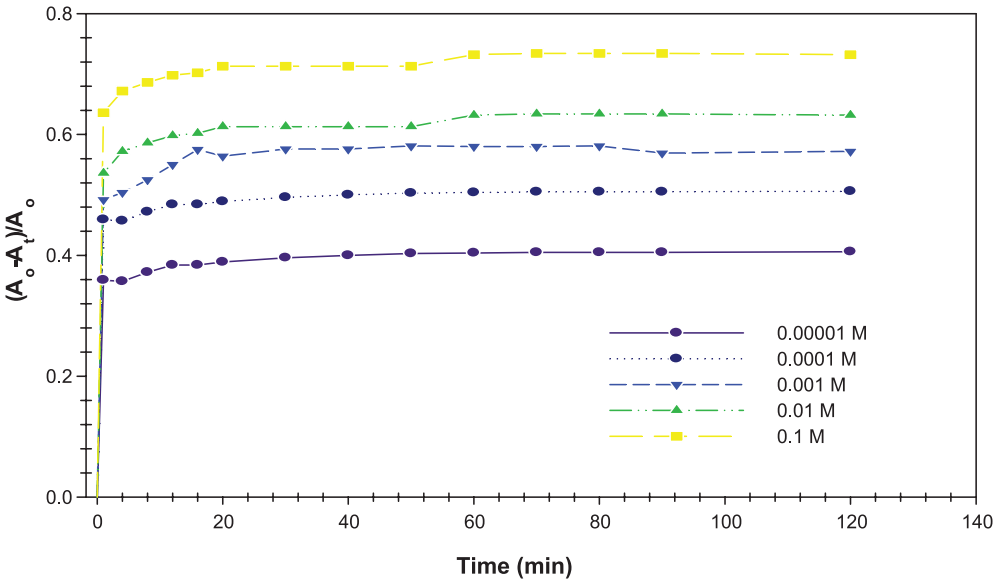

Figure 9. Relative change of the absorbance strength of the Acacia gum–stabilised silver nanoparticles with different concentrations of H_2O_2 solution at different time intervals (0-120 minutes).

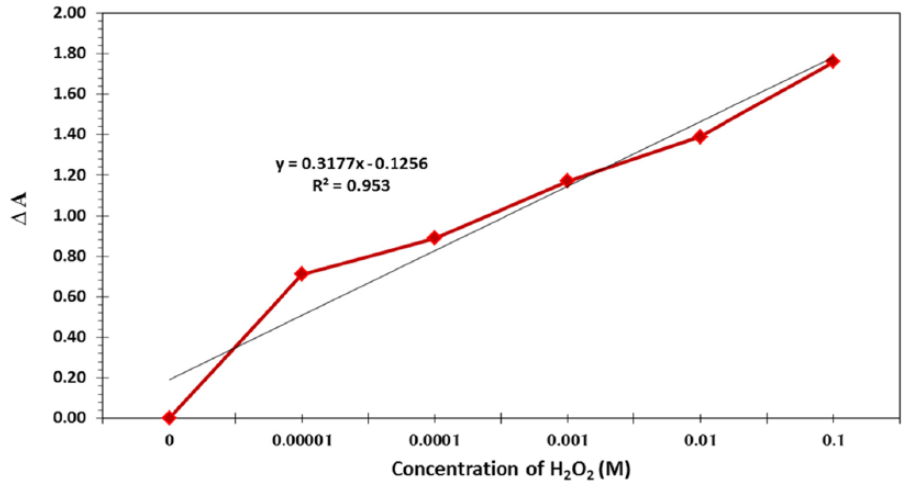

Figure 10. Calibration curve of H_2O_2 from 0.1 to 0.00001 M using Acacia gum–stabilised silver nanoparticle–based localised surface plasmon resonance colorimetric sensor.

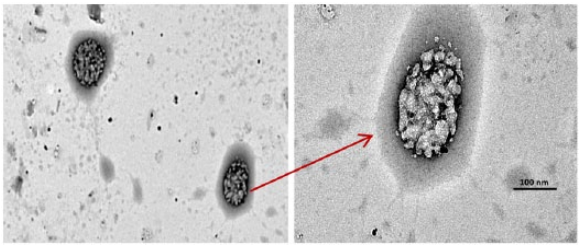

Figure 11. Transmission electron microscopy micrographs of Acacia gum–stabilised silver nanoparticles after introducing 0.001 M hydrogen peroxide solution.

solution, the Acacia gum–stabilised SNPs were stable and dispersed in the dispersion medium, resulting in effective excitation of the LSPR band absorbance. On the contrary, when H_2O_2 solution was added to the Acacia gum–stabilised SNPs, the nanoparticles were aggregated by the catalytic reaction between SNPs and H_2O_2 solution, and the aggregation of nanoparticles causes the LSPR band absorbance strength to decrease.[63,64]

Investigation with a real sample

To investigate the actual applicability of the fabricated SNPs for real sample analysis, two different types of liquid milk samples (Almarai and Alsafi) where chosen as real samples; 5×10^{-3} and 2×10^{-4} M H_2O_2 solution was added to Acacia gum–stabilised SNPs at a ratio of 1:1.5, and the solutions were subsequently analysed using a UV-Vis spectrophotometer. As can be seen in Table 2, the milk sample without spiked H_2O_2 solution did not provide any detectable signal, whereas the recovery for the H_2O_2 solution was found to be more than 97%, with an RSD of less than 6% (n = 3). This result shows that the proposed procedure was suitable for measuring H_2O_2 solution in liquid milk samples.

Table 1. The intraday and interday precision (n = 3) of the analysis of 0.001 M H_2O_2 solution in triplicate analyses.

INTRADAY PRECISION	INTERDAY PRECISION
3.1	5.9
4.7	3.5
4.4	6.4

Conclusions

In the present investigation, Acacia gum–stabilised SNPs were fabricated through a rapid, simple, eco-friendly, and economically sustainable green method to synthesise SNPs using white sugar as a reducing reagent, Acacia gum as a stabilising agent, and NaOH as a reaction accelerator. The fabricated Acacia gum–stabilised SNPs in this study had an LSPR band at 407 nm and high colloidal stability. Moreover, the chemical composition, morphology, and physical and thermal properties of the fabricated nanoparticles were characterised using different techniques. The results of the TEM micrographs confirmed that the fabricated nanoparticles were in the nano range and that they were spherical with a narrow size distribution and average diameter of 10 nm. The Acacia gum–stabilised SNPs were used for the detection of an H_2O_2 solution, which was monitored using spectrophotometry. The results demonstrated that the LSPR optical characteristics drastically changed after adding H_2O_2 to the Acacia gum–stabilised SNP solution depending on the concentration of H_2O_2, caused by the degradation of SNPs induced by the catalytic decomposition of H_2O_2. From these characteristics, this LSPR-based optical sensor for the detection of H_2O_2 using the fabricated nanoparticles was shown to be a fast, simple, and cost-effective method that could be applied as a colour indicator in different applications of industrial, medical, and environmental research.

Table 2. Recovery experiments for determination of H_2O_2 in real sample (n = 3).

SAMPLE	FOUND (M)	SPIKED (M)	FOUND (M)	RECOVERY (%)	RSD (%)
Milk (Almarai)	Not detected	5×10^{-3}	4.9×10^{-3}	98	4.7
Milk (Alsafi)	Not detected	2×10^{-4}	1.95×10^{-4}	97.5	5.3

Abbreviation: RSD, relative standard deviation.

REFERENCES

1. Alzahrani E, Welham K. Optimization preparation of the biosynthesis of silver nanoparticles using watermelon and study of itsantibacterial activity. *Int J Basic Appl Sci*. 2014;3:392–400.
2. Sørensen SN, Baun A. Controlling silver nanoparticle exposure in algal toxicity testing – a matter of timing. *Nanotoxicology*. 2015;9:201–209.
3. Pluháček T, Lemr K, Ghosh D, Milde D, Novák J, Havlíček V. Characterization of microbial siderophores by mass spectrometry. *Mass Spectrom Rev*. 2016;35:35–47.
4. Bhainsa KC, D'souza S. Extracellular biosynthesis of silver nanoparticles using the fungus Aspergillus fumigatus. *Colloids Surf B: Biointerfaces*. 2006;47:160–164.
5. Andrade FAC, de Oliveira Vercik LC, Monteiro FJ, da Silva Rigo EC. Preparation, characterization and antibacterial properties of silver nanoparticles–hydroxyapatite composites by a simple and eco-friendly method. *Ceram Int*. 2016;42:2271–2280.
6. Kobayashi Y, Katakami H, Mine E, Nagao D, Konno M, Liz-Marzán LM. Silica coating of silver nanoparticles using a modified Stöber method. *J Colloid Interf Sci*. 2005;283:392–396.
7. Willander M, Nur O, Lozovik YE, et al. Solid and soft nanostructured materials: fundamentals and applications. *Microelectr J*. 2005;36:940–949.
8. Alzahrani E. Eco-friendly production of silver nanoparticles from peel of tangerine for degradation of dye. *World J Nanosci Eng*. 2015;5:10–16.
9. Sherry LJ, Jin R, Mirkin CA, Schatz GC, Van Duyne RP. Localized surface plasmon resonance spectroscopy of single silver triangular nanoprisms. *Nano Lett*. 2006;6:2060–2065.
10. Endo T, Ikeda R, Yanagida Y, Hatsuzawa T. Stimuli-responsive hydrogel–silver nanoparticles composite for development of localized surface plasmon resonance-based optical biosensor. *Anal Chim Acta*. 2008;611:205–211.
11. Endo T, Kerman K, Nagatani N, Takamura Y, Tamiya E. Label-free detection of peptide nucleic acid-DNA hybridization using localized surface plasmon resonance based optical biosensor. *Anal Chem*. 2005;77:6976–6984.
12. Willets KA, Van Duyne RP. Localized surface plasmon resonance spectroscopy and sensing. *Annu Rev Phys Chem*. 2007;58:267–297.
13. Endo T, Kerman K, Nagatani N, et al. Multiple label-free detection of antigen-antibody reaction using localized surface plasmon resonance-based core-shell structured nanoparticle layer nanochip. *Anal Chem*. 2006;78:6465–6475.
14. Cooke MS, Olinski R, Evans MD. Does measurement of oxidative damage to DNA have clinical significance? *Clin Chim Acta*. 2006;365:30–49.
15. Kuisma M, Sakko A, Rossi TP, et al. Localized surface plasmon resonance in silver nanoparticles: atomistic first-principles time-dependent density-functional theory calculations. *Phys Rev B*. 2015;91:1–8.
16. Shrivas K, Sahu S, Patra GK, Jaiswal NK, Shankar R. Localized surface plasmon resonance of silver nanoparticles for sensitive colorimetric detection of chromium in surface water, industrial waste water and vegetable samples. *Anal Method*. 2016;8:2088–2096.
17. Filippo E, Serra A, Manno D. Poly (vinyl alcohol) capped silver nanoparticles as localized surface plasmon resonance-based hydrogen peroxide sensor. *Sensor Actuat B: Chem*. 2009;138:625–630.
18. Endo T, Yanagida Y, Hatsuzawa T. Quantitative determination of hydrogen peroxide using polymer coated Ag nanoparticles. *Measurement*. 2008;41:1045–1053.
19. Tashkhourian J, Hormozi-Nezhad MR, Khodaveisi J, Dashti R. Localized surface plasmon resonance sensor for simultaneous kinetic determination of peroxyacetic acid and hydrogen peroxide. *Anal Chim Acta*. 2013;762:87–93.
20. Pastoriza-Santos I, Liz-Marzán LM. Formation and stabilization of silver nanoparticles through reduction by N, N-dimethylformamide. *Langmuir*. 1999;15:948–951.
21. Iravani S, Korbekandi H, Mirmohammadi S, Zolfaghari B. Synthesis of silver nanoparticles: chemical, physical and biological methods. *Res Pharm Sci*. 2014;9:385–406.
22. Ahmad T, Wani IA, Khatoon S. Controlling the size and morphology of silver nanoparticles: role of chemical routes. *Nanotech*. 2011;292–298.
23. Sun Y-P, Atorngitjawat P, Meziani MJ. Preparation of silver nanoparticles via rapid expansion of water in carbon dioxide microemulsion into reductant solution. *Langmuir*. 2001;17:5707–5710.
24. Henglein A. Physicochemical properties of small metal particles in solution: 'microelectrode' reactions, chemisorption, composite metal particles, and the atom-to-metal transition. *J Phys Chem*. 1993;97:5457–5471.
25. Ponarulselvam S, Panneerselvam C, Murugan K, Aarthi N, Kalimuthu K, Thangamani S. Synthesis of silver nanoparticles using leaves of Catharanthus roseus Linn. G. Don and their antiplasmodial activities. *Asian Pac J Trop Biomed*. 2012;2:574–580.
26. Konishi Y, Ohno K, Saitoh N, et al. Bioreductive deposition of platinum nanoparticles on the bacterium Shewanella algae. *J Biotechnol*. 2007;128:648–653.
27. Prabhu S, Poulose EK. Silver nanoparticles: mechanism of antimicrobial action, synthesis, medical applications, and toxicity effects. *Int Nano Lett*. 2012;2:1–10.
28. Willner I, Baron R, Willner B. Growing metal nanoparticles by enzymes. *Adv Mater*. 2006;18:1109–1120.
29. Zhang X, He X, Wang K, Yang X. Different active biomolecules involved in biosynthesis of gold nanoparticles by three fungus species. *J Biomed Nanotechnol*. 2011;7:245–254.
30. Jain D, Daima HK, Kachhwaha S, Kothari S. Synthesis of plant-mediated silver nanoparticles using papaya fruit extract and evaluation of their anti microbial activities. *Dig J Nanomater Bios*. 2009;4:557–563.
31. Saxena A, Tripathi R, Singh R. Biological synthesis of silver nanoparticles by using onion (Allium cepa) extract and their antibacterial activity. *Dig J Nanomater Bios*. 2010;5:427–432.
32. Geetha N, Harini K, Showmya JJ, Priya KS. Biofabrication of silver nanoparticles using leaf extract of Chromolaena odorata (L.) King and Robinson. In: Proceedings of the International Conference on Nuclear Energy, Environmental and Biological Sciences; September 8-9, 2012:56–59; Bangkok, Thailand.
33. Ahmed S, Ahmad M, Swami BL, Ikram S. A review on plants extract mediated synthesis of silver nanoparticles for antimicrobial applications: a green expertise. *J Adv Res*. 2016;7:17–28.
34. Srikar SK, Giri DD, Pal DB, Mishra PK, Upadhyay SN. Green synthesis of silver nanoparticles: a review. *Green Sustain Chem*. 2016;6:34–56.
35. Altantzis T, Yang Z, Bals S, Van Tendeloo G, Pileni M-P. Thermal stability of CoAu13 binary nanoparticle superlattices under the electron beam. *Chem Mater*. 2016;28:716–719.
36. Rajan K, Roppolo I, Chiappone A, Bocchini S, Perrone D, Chiolerio A. Silver nanoparticle ink technology: state of the art. *Nanotechnol Sci Appl*. 2016;9:1–13.
37. Swain B, Mishra C, Hong HS, Cho S-S. Selective recovery of pure copper nanopowder from indium-tin-oxide etching wastewater by various wet chemical reduction process: understanding their chemistry and comparisons of sustainable valorization processes. *Environ Res*. 2016;147:249–258.
38. Oliveira MM, Ugarte D, Zanchet D, Zarbin AJ. Influence of synthetic parameters on the size, structure, and stability of dodecanethiol-stabilized silver nanoparticles. *J Colloid Interface Sci*. 2005;292:429–435.
39. Vasileva P, Donkova B, Karadjova I, Dushkin C. Synthesis of starch-stabilized silver nanoparticles and their application as a surface plasmon resonance-based sensor of hydrogen peroxide. *Colloid Surface A*. 2011;382:203–210.
40. Abdel-Hafez SI, Nafady NA, Abdel-Rahim IR, Shaltout AM, Mohamed MA. Biogenesis and optimisation of silver nanoparticles by the endophytic fungus Cladosporium sphaerospermum. *Int J Nanostruct Chem*. 2016;2:11–19.
41. Krupa AND, Abigail MEA, Santhosh C, Grace AN, Vimala R. Optimization of process parameters for the microbial synthesis of silver nanoparticles using 3-level Box–Behnken Design. *Ecol Eng*. 2016;87:168–174.
42. Mosae Selvakumar P, Antonyraj CA, Babu R, Dakhsinamurthy A, Manikandan N, Palanivel A. Green synthesis and antimicrobial activity of monodispersed silver nanoparticles synthesized using lemon extract. *Synth React Inorg Me*. 2016;46:291–294.
43. Lee E-J, Piao L, Kim J-K. Synthesis of silver nanoparticles from the decomposition of silver (I) [bis (alkylthio) methylene] malonate complexes. *B Kor Chem Soc*. 2012;33:60–64.
44. Hou W, Cronin SB. A review of surface plasmon resonance-enhanced photocatalysis. *Adv Funct Mater*. 2013;23:1612–1619.
45. Rahimi G, Alizadeh F, Khodavandi A. Mycosynthesis of silver nanoparticles from Candida albicans and its antibacterial activity against Escherichia coli and Staphylococcus aureus. *Trop J Pharm Res*. 2016;15:371–375.

46. Agnihotri S, Mukherji S, Mukherji S. Size-controlled silver nanoparticles synthesized over the range 5-100 nm using the same protocol and their antibacterial efficacy. *RSC Adv*. 2014;4:3974–3983.
47. Chairam S, Somsook E. Starch vermicelli template for synthesis of magnetic iron oxide nanoclusters. *J Magn Magn Mater*. 2008;320:2039–2043.
48. Tai CY, Wang YH, Liu HS. A green process for preparing silver nanoparticles using spinning disk reactor. *AIChE J*. 2008;54:445–452.
49. Chairam S, Poolperm C, Somsook E. Starch vermicelli template-assisted synthesis of size/shape-controlled nanoparticles. *Carbohyd Polym*. 2009; 75:694–704.
50. Kelly KL, Coronado E, Zhao LL, Schatz GC. The optical properties of metal nanoparticles: the influence of size, shape, and dielectric environment. *J Phys Chem B*. 2003;107:668–677.
51. Wilcoxon JP, Abrams BL. Synthesis, structure and properties of metal nanoclusters. *Chem Soc Rev*. 2006;35:1162–1194.
52. Martinez-Castanon G, Nino-Martinez N, Martinez-Gutierrez F, Martinez-Mendoza J, Ruiz F. Synthesis and antibacterial activity of silver nanoparticles with different sizes. *J Nanopart Res*. 2008;10:1343–1348.
53. Bar H, Bhui DK, Sahoo GP, Sarkar P, De SP, Misra A. Green synthesis of silver nanoparticles using latex of Jatropha curcas. *Colloid Surface A*. 2009;339: 134–139.
54. Govindarajan M, Rajeswary M, Veerakumar K, Muthukumaran U, Hoti S, Benelli G. Green synthesis and characterization of silver nanoparticles fabricated using Anisomeles indica: mosquitocidal potential against malaria, dengue and Japanese encephalitis vectors. *Exp Parasitol*. 2016;161:40–47.
55. Murugan K, Raman C, Panneerselvam C, et al. Nano-insecticides for the control of human and crop pests. In: Raman C, Goldsmith MR, Agunbiade TA, eds. *Short Views on Insect Genomics and Proteomics*. New York: Springer; 2016:229–251.
56. Puchalski M, Dąbrowski P, Olejniczak W, Krukowski P, Kowalczyk P, Polański K. The study of silver nanoparticles by scanning electron microscopy, energy dispersive X-ray analysis and scanning tunnelling microscopy. *Mater Sci: Poland*. 2007;25:473–478.
57. Picart C, Schneider A, Etienne O, et al. Controlled degradability of polysaccharide multilayer films in vitro and in vivo. *Adv Funct Mater*. 2005;15:1771–1780.
58. Rao Y, Banerjee D, Datta A, Das S, Guin R, Saha A. Gamma irradiation route to synthesis of highly re-dispersible natural polymer capped silver nanoparticles. *Radiat Phys Chem*. 2010;79:1240–1246.
59. Chang PR, Jian R, Yu J, Ma X. Fabrication and characterisation of chitosan nanoparticles/plasticised-starch composites. *Food Chem*. 2010;120:736–740.
60. Chang PR, Yu J, Ma X, Anderson DP. Polysaccharides as stabilizers for the synthesis of magnetic nanoparticles. *Carbohyd Polym*. 2011;83:640–644.
61. Park J-H, Byun J-Y, Yim S-Y, Kim M-G. A Localized Surface Plasmon Resonance (LSPR)-based, simple, receptor-free and regeneratable Hg2+ detection system. *J Hazard Mater*. 2016;307:137–144.
62. Ringe E, McMahon JM, Sohn K, et al. Unraveling the effects of size, composition, and substrate on the localized surface plasmon resonance frequencies of gold and silver nanocubes: a systematic single-particle approach. *J Phys Chem C*. 2010;114:12511–12516.
63. Zhang Q, Cobley CM, Zeng J, Wen L-P, Chen J, Xia Y. Dissolving Ag from Au–Ag alloy nanoboxes with H_2O_2: a method for both tailoring the optical properties and measuring the H_2O_2 concentration. *J Phys Chem C*. 2010;114: 6396–6400.
64. Amirjani A, Bagheri M, Heydari M, Hesaraki S. Label-free surface plasmon resonance detection of hydrogen peroxide: a bio-inspired approach. *Sensor Actuat B: Chem*. 2016;227:373–382.
65. Tagad CK, Dugasani SR, Aiyer R, Park S, Kulkarni A, Sabharwal S. Green synthesis of silver nanoparticles and their application for the development of optical fiber based hydrogen peroxide sensor. *Sensor Actuat B: Chem*. 2013;183:144–149.
66. Zhang Y, McKelvie ID, Cattrall RW, Kolev SD. Colorimetric detection based on localised surface plasmon resonance of gold nanoparticles: merits, inherent shortcomings and future prospects. *Talanta*. 2016;152:410–422.
67. Shrivas K, Shankar R, Dewangan K. Gold nanoparticles as a localized surface plasmon resonance based chemical sensor for on-site colorimetric detection of arsenic in water samples. *Sensor Actuat B: Chem*. 2015;220:1376–1383.